ARTICLE

Check for updates

Tunable single-mode chip-scale mid-infrared laser

Euijae Shim[1✉], Andres Gil-Molina [1], Ohad Westreich[1], Yamac Dikmelik[2], Kevin Lascola[2], Alexander L. Gaeta[3] & Michal Lipson [1✉]

Portable mid-infrared (mid-IR) spectroscopy and sensing applications require widely tunable, chip-scale, single-mode sources without sacrificing significant output power. However, no such lasers have been demonstrated beyond 3 μm due to the challenge of building tunable, high quality-factor (Q) on-chip cavities. Here we demonstrate a tunable, single-mode mid-IR laser at 3.4 μm using a tunable high-Q silicon microring cavity and a multi-mode Interband Cascade Laser. We achieve single-frequency lasing with 0.4 mW output power via self-injection locking and a wide tuning range of 54 nm with 3 dB output power variation. We further estimate an upper-bound effective linewidth of 9.1 MHz and a side mode suppression ratio of 25 dB from the locked laser using a scanning Fabry-Perot interferometer. Our laser platform based on a tunable high-Q microresonator can be expanded to higher wavelength quantum-cascade lasers and lead to the development of compact, high-performance mid-IR sensors for spectroscopic applications.

[1] Department of Electrical Engineering, Columbia University, New York, NY 10027, USA. [2] Thorlabs, Inc., Newton, NJ, USA. [3] Department of Applied Physics and Applied Mathematics, Columbia University, New York, NY 10027, USA. ✉email: es3500@columbia.edu; ml3745@columbia.edu

Chip-scale, widely tunable, narrow-linewidth lasers in the mid-infrared (mid-IR) are critical for a variety of sensing and spectroscopic applications. The 3–5 μm wavelength range is of particular interest for biomedical and environmental gas sensing since this region is the Earth's transparency window where important greenhouse gases and hydrocarbons have their strong absorption signatures[1]. Tunable narrow-linewidth lasers must be developed to achieve fast and precise spectroscopy of gas-phase molecules that are typically narrower than 1 GHz[1]. The goal is to build compact, field-deployable sensors with high-performance chip-scale lasers. Such lasers beyond 3 μm wavelength, however, have not been developed up to this point in time. Previous work includes distributed feedback-Quantum/Interband Cascade lasers (DFB-QCL/ICL)[2–4] that can provide high-power and single-mode output for compact mid-IR applications, but wavelength tuning of these lasers is achieved at the cost of significant output power variation related to direct tuning of gain medium. Mid-IR tunable lasers based on external cavities have been demonstrated[5–7] but the bulky free-space external cavities make their miniaturization challenging. V-shaped coupling of two Fabry–Perot (FP) cavities inside an ICL for single-mode lasing and wide tunability at 2.8 μm[8] was recently studied to address these challenges. This approach, however, introduces significant complexity, requiring full customization and fabrication of the laser diode.

Building high-performance, chip-scale mid-IR lasers requires the design and development of high quality factor (Q) on-chip cavities in the mid-IR. While chip-scale lasers with frequency tunability and narrow linewidth have been demonstrated using high-Q on-chip cavities[9–11] in the near-IR (NIR), enabling on-chip optical frequency combs[12,13], there is no comparable demonstrations for the mid-IR range. Specifically, engineering tunable high-Q on-chip cavities beyond 3 μm is difficult due to the lack of appropriate tunable transparent materials. Conventional transparent materials in the mid-IR are either not tunable (e.g. fluoride crystallines and chalcogenide glasses[14]) or require customized complex material fabrication such as high-quality molecular-beam epitaxial process (e.g. germanium-on-silicon[15,16]).

Here we demonstrate a tunable single-mode mid-IR laser that uses a high-Q silicon-chip microresonator for self-injection locking of an ICL. Our mid-IR laser design induces spatial collapse of the multi-mode ICL into a single-mode by tuning the ring resonance into one of the ICL modes. To tune the cavity, we employ silicon's thermo-optic effect by leveraging the full CMOS fabrication infrastructure of silicon photonics that provides a compact, chip-scale solution.

Results and discussion

A schematic of our single-frequency mid-IR laser is shown in Fig. 1a, and the microscope image of the silicon chip is shown in Fig. 1b. A detailed schematic of the operation principle of the single-mode laser is shown in Fig. 1c. In contrast to other laser configurations that leverage the optical feedback to the laser diode or gain chip using backward Rayleigh scattering of the resonators[9–11], we design a microresonator integrated with an external Sagnac reflector where one can control the strength of reflection for optical feedback to the Fabry–Perot ICL. The reflection of the Sagnac reflector is designed to be above 99 % as shown in Fig. 1d. In this way, we ensure strong optical feedback without relying on the amount of scattering of the resonator[17]. Since a circulator, required for reflectivity measurement is not commercially available in this mid-IR wavelength range, we estimate the impact of fabrication-induced variations on the reflectance. The Sagnac loop mirror structure includes a gap of

400 nm between two waveguides, fabricated with high precision using an electron-beam lithography tool (8 nm resolution Elionix ELS-G100). A ± 10 nm variation of the gap size would result in 97.7–99.9% reflection according to Lumerical Finite Difference Eigenmode (FDE) simulations. Therefore, the degree of fabrication variation should have minimal impact on the reflectance.

We engineer a mid-IR on-chip silicon waveguide ring cavity with high-$Q > 10^5$ so that only a single-mode propagates in each direction. In order to simultaneously achieve high-Q cavity for high frequency selectivity and tunability, we deposit 2 μm of oxide on the silicon waveguide to isolate the mode from the lossy metal used for the microheaters and design the optical mode to minimally overlap with the absorbing oxide. The silicon waveguide [2000 nm (H) × 2400 nm (W)] is optimized for strong confinement of the fundamental TE mode with a calculated absorption-limited propagation loss of 0.25 dB/cm. We ensure that only a single-mode is fed back to the ICL, despite the fact that the microresonator supports multi-transverse modes, by designing the coupling regions between the microresonator and the Sagnac reflector to be phase-matched only for the fundamental TE. Figure 2a shows the simulated mode profile of the silicon waveguide for a 150-μm radius ring. We experimentally estimate the Q of the microresonator by measuring the transmission spectrum using a tunable optical parametric oscillator (OPO) source near 3.4 μm. Figure 2b shows the transmission spectrum of the microresonator with a linewidth of 323 MHz, corresponding to a loaded Q of 2.8×10^5.

To ensure the dominance of the reflections from the Sagnac reflector ($\approx$99%) over undesirable reflections, we use a high-aspect-ratio inverse taper. To couple light out of the chip, we design the inverse taper to become delocalized so that the effective index is much lower ($\approx$1.459) at 3.4 μm. This lower index decreases Fresnel reflections of a typical silicon-air interface of 30 % down to 3%. Figure 3a illustrates the high-aspect-ratio inverse taper, and Fig. 3b shows the mode profile of the inverse taper for fundamental TE mode. We describe chip fabrication in Methods. Figure 3c shows the SEM image of the inverse taper structure fabricated on a silicon chip. Our suspended inverse taper is designed to be robust to any mechanical vibrations by fabricating anchors to the 4 μm of top and bottom oxide cladding. In addition to ensuring low reflections of the output facet, we also design the waveguide to ensure low reflections at the input facet. To decrease Fresnel reflections at the input facet from 30% to 17%, we design a Si/SiO$_2$ faceted horn taper with a mode distribution that matches the ICL fundamental mode and clad the taper facet by several microns of SiO$_2$. To prevent leakage of light into the silicon substrate through the 2 μm-thick buried oxide layer, we etch the silicon substrate under the input taper region at the edge of the silicon chip over a length of 5 μm.

We show single-mode lasing with up to 0.4 mW of output power via self-injection locking of the multi-mode ICL. We observe in Fig. 4b the optical spectrum of the unlocked free-running multi-mode ICL when no power is applied to integrated heaters [see Fig. 4a], and the ring resonance is off resonance with ICL modes. Figure 4d shows the optical spectrum of injection locked ICL when power is applied to integrated heaters that tune the ring resonance and the phase of the adjacent waveguide [see Fig. 4c]. Tuning ensures high reflectivity and constructive interference between the external cavity mode and the ICL mode, leading to the collapse of the ICL multi-mode spectrum into a single-mode. Figure 4d shows that the locked-state power is higher than that of the highest power in the free-running state by at least 6 dB, additional evidence of typical mode collapse[18]. In this high-power mode collapse, the power of the ICL is redistributed in favor of the locked mode and therefore can be easily distinguished from a simple frequency filtering effect.
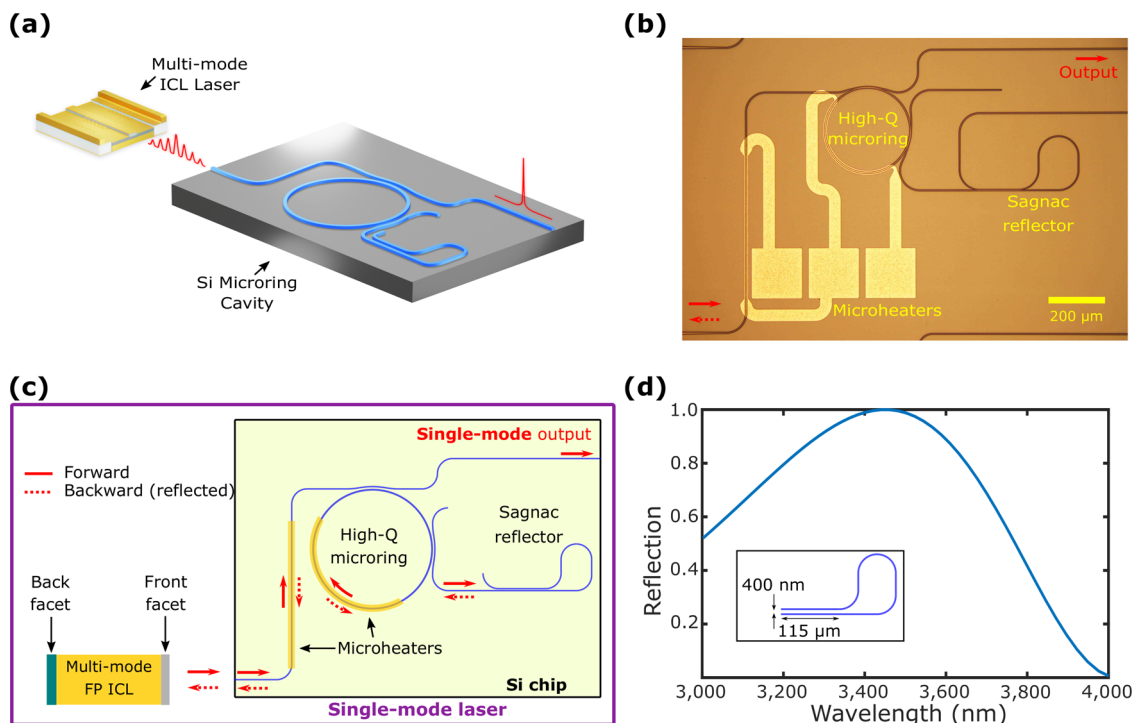
Fig. 1 Single-mode laser platform by integrating a multi-mode Fabry–Perot (FP) interband cascade laser (ICL) laser with a high quality factor (Q) microresonator. a Illustration of a single-frequency mid-IR source, consisting of a multi- mode ICL laser and a silicon microring cavity. **b** Microscope image of the silicon chip with a 150-μm radius high-Q microring (coupling gap of 510 nm), a Sagnac reflector, and aluminum microheaters. **c** Schematic of the single-mode laser. A multi-mode ICL around 3.4 μm with an anti-reflection coating on the front facet. The Sagnac reflector at the drop port provides frequency-selective optical feedback and form an external cavity with the ICL back facet. Microheaters are placed on top of the bus waveguide and the microring to control the phase of the external cavity and the ring resonance, respectively. **d** Simulated reflection spectrum of the Sagnac loop mirror over wavelengths from 3 μm to 4 μm using Finite-Difference Eigenmode solver. The Sagnac loop mirror reflects about 99% at the drop port at 3.4 μm. A coupler of the Sagnac loop mirror at the drop port consists of a 400 nm gap and a 115 μm length.
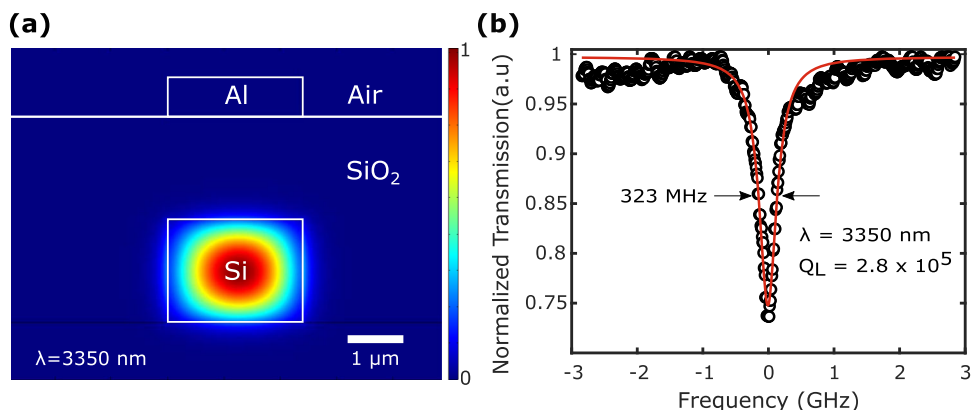

Fig. 2 Mode simulation and normalized transmission spectrum of the fundamental transverse electric (TE) mode at 3350 nm. a Finite Element Mode (FEM) simulation of the fundamental TE mode for a silicon waveguide (2000 nm height (H) × 2400 nm width (W)) with oxide cladding and aluminum (Al) heater on top for a 150 μm bending radius. **b** Transmission spectrum of the microring at 3350 nm wavelength (λ) measured using a piezo controlled optical parametric oscillator (OPO) system. The measured linewidth is 323 MHz, corresponding to the loaded quality factor (Q_L) of 2.8×10^5.

The wavelength of the locked laser is stable for hours, evidenced by the scanning Fabry–Perot interferometer measurement with a ms-scale time response. We do not observe any deviation of the lasing wavelength within the interferometer resolution of 9.1 MHz.

Our mid-IR laser demonstrates a 54-nm-wide tuning range of lasing wavelength from 3367 nm to 3421 nm. Figure 5 shows the tuning of the single-frequency state in the optical spectrum. We tune the wavelength of a single-frequency state by tuning both the ring (to ensure that the resonance matches with one of the FP ICL

modes) and the phase of the adjacent waveguide (to ensure that there is no external cavity net phase accumulated per round trip) by applying less than 100 mW of electrical power to the integrated heaters on top of the bus and ring waveguides. For the spectra of Fig. 5 we apply a diode current of 402 mA (±10%) at the diode temperature of 22 °C (±0.5 C). These slight variations of the laser diode operation point allowed us to tune the gain spectrum, enabling wide tunability with a low output power variation of 3 dB. Note that our approach for wide tuning of lasing wavelength is controlled by the microresonator resonance
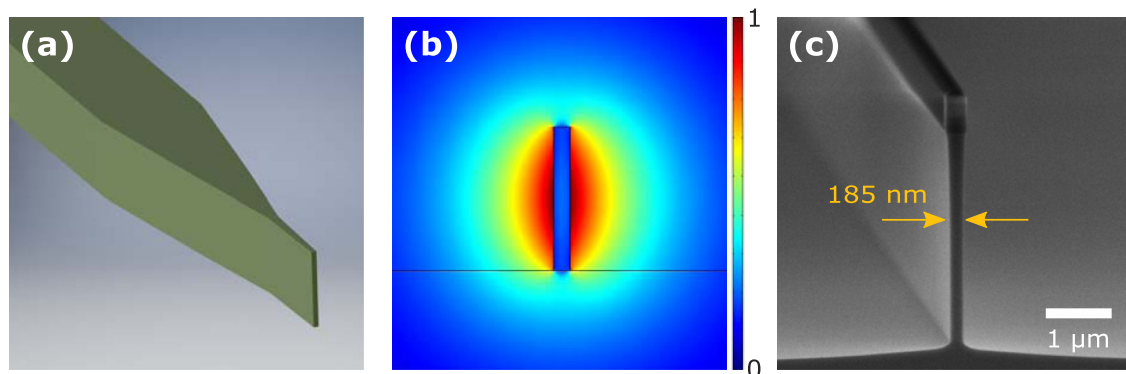
Fig. 3 Design and microscope image of the inverse taper. a Illustration of the inverse taper used to minimize reflections at the output facet. **b** Finite Element Mode (FEM) simulation of the fundamental transverse electric (TE) mode of the inverse taper with 2000 nm height (H) × 200 nm width (W). **c** Scanning electron microscope (SEM) image of a high-aspect-ratio inverse taper structure similar to the one used in our mid-infrared (mid-IR) laser.
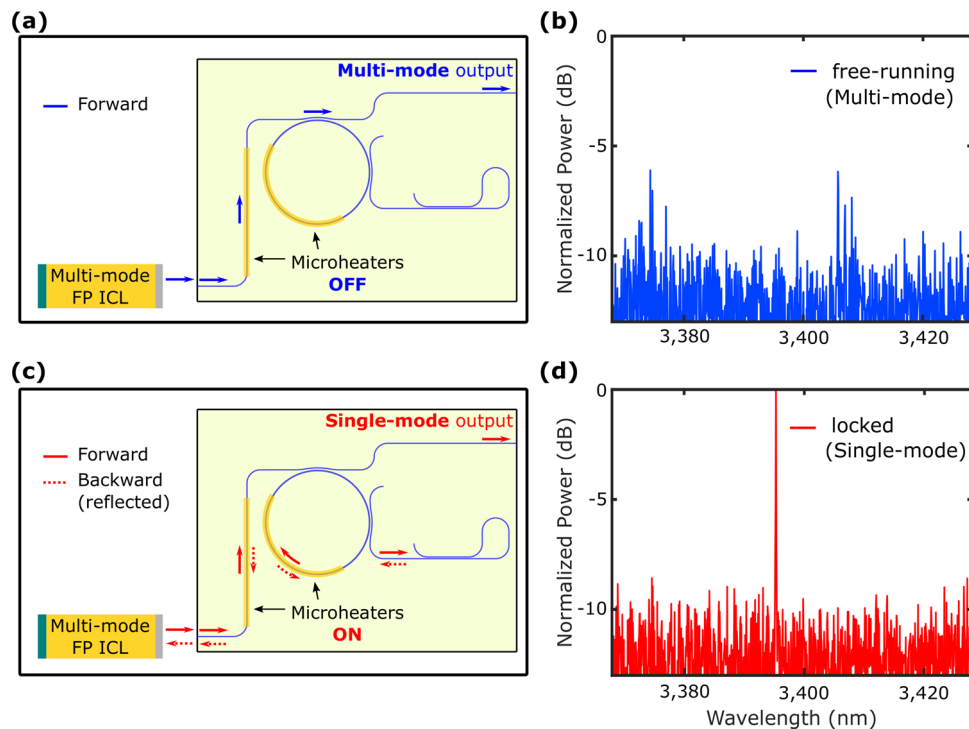
Fig. 4 Self-injection locking of a Fabry–Perot (FP) interband cascade laser (ICL) diode by a microresonator with integrated heaters. a Schematic of the laser setup where microheaters are turned off, and the ring is off-resonance. **b** Optical spectrum of the free-running state laser with multi-mode output. **c** Schematic of the laser setup where microheaters are turned on, and the ring is on-resonance. **d** Optical spectrum of the single-mode locked-state laser. The power measured at the output facet of the chip through an aspheric lens is 0.4 mW near the wavelength of 3.4 μm. laser.

frequencies in contrast to the typical thermo-optic tuning of the gain medium in DFB lasers which inevitably results in higher output power variation over a tuning range. The maximum current applied to the ICL diode in this work is 443 mA close to the recommended maximum current of 470 mA, indicating that our results correspond to the high power regime of the ICL. For lower pump current, on the other hand, the laser locking can easily be achieved as there are fewer modes involved in the competition for gain in the ICL. The tuning range is limited by the gain bandwidth of the ICL and the coupling efficiency between the ICL and the chip. We attribute the power drop in the middle wavelengths in Fig. 5 to the gain medium profile of the ICL, indicating that the ICL can lase in the locked state (single-frequency) for most of the gain bandwidth.
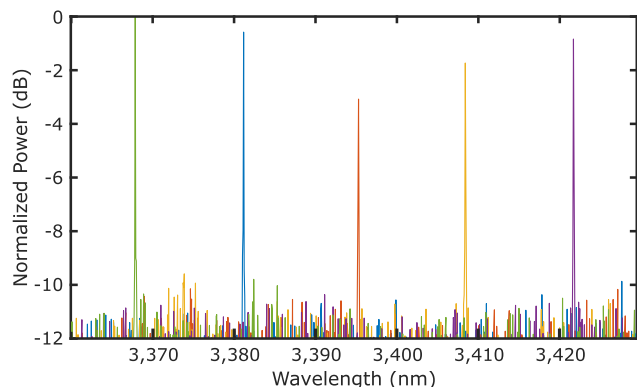
We estimate an upper-bound the effective linewidth of 9.1 MHz of the locked laser limited by the resolution of the

interferometer. We show the schematic of our experimental setup in Fig. 6a and linewidth measurement in Fig. 6b. The locked laser beam is aligned to the interferometer using a pair of irises and collected at a photodetector; the interferometer resonance is scanned with a piezoelectric controller. We estimate the fundamental linewidth (Schawlow–Townes linewidth) of the locked laser to be $\Delta\nu_{locked} \approx 580$ Hz, excluding any source of technical noise and assuming an output power equal to the measured value of 0.4 mW, and coupling loss and quality factor values similar to those in our experiments. Figure 6c shows the calculated fundamental linewidth versus loaded quality factor for different coupling losses between the ICL and the silicon chip. We show that the fundamental linewidth can be further reduced to Hz-level by using a silicon resonator with a Q of 10^6 and improved coupling loss of 3 dB. Further details of linewidth estimation are discussed in Methods. Figure 6d shows the measured side mode

suppression ratio (SMSR) of 25 dB of the locked-state laser, limited by the oscilloscope's sensitivity. When the interferometer is scanned over 2 GHz (greater than the interferometer's FSR of 1.5 GHz), we observe no side-bands of the locked-state ICL, giving further evidence of self-injection locking of the ICL.

In summary, we demonstrate a high-Q tunable microresonator integrated with an off-the-shelf ICL/QCL diode platform for realizing widely tunable, chip-scale, and single-mode lasers beyond 3 μm. Table 1 shows the performance metrics of chip-scale ICLs near 3.0 μm wavelength. While single-mode ICLs operating beyond 3 μm are commercially available, these DFB

Fig. 5 Tuning of the lasing wavelength in the locked-state laser. Optical spectra showing the wide tunability of the locked-state laser of over 54 nm in wavelength near 3.4 μm. Green, blue, orange, yellow, and purple lines represent lasing wavelength tuning for 0 mW, 24 mW, 37 mW, 66 mW, and 99 mW of electrical power applied to the microheater on top of the ring resonator, respectively. In addition, less than 100 mW of electrical power was applied to the microheater on top of the adjacent bus waveguide for phase matching.

lasers show limited tunability due to their reliance on thermal tuning of the active medium. Our laser design has significant implications for the development of chip-scale spectrometers and gas sensors in the mid-IR since it does not require complex material fabrication or bulky external cavities. In addition, our self-injection locking based approach can be applied to other types of laser cavities as shown in NIR[10,19] such as DFB types at wavelengths up to 8 μm limited by the transparency window of silicon waveguides. Further linewidth reduction of a mid-IR laser diode can be achieved by integrating a higher Q microresonator like our recently demonstrated $Q = 10^6$ air-clad silicon microresonator[20] whose resonance and phase can, in principle, be controlled by placing microheaters on the side of waveguides. Combined with microresonator-based mid-IR combs[21,22] and commercially available higher power ICL/QCLs, our approach paves the way for compact comb-based spectroscopy in the 3–5 μm wavelength region and beyond.

Methods

Fabrication. We fabricate the oxide-clad silicon microring resonator and waveguides with integrated heaters using standard CMOS manufacturing processes. We start with a silicon on insulator wafer with 2 μm oxide and 2 μm silicon layer thicknesses. To fully etch the 2 μm thick silicon layer with a small coupling gap between the ring and the bus waveguide, we spin ma-N 2410 electron beam resist on the wafer to form a 1.5 μm thick resist layer. To reduce the sidewall roughness, we pattern waveguides using multi-pass e-beam lithography followed by an inductively coupled plasma dry etching based on C_4F_8 and SF_6. After cleaning the wafer with Piranha etchant, we deposit a 2 μm oxide layer using plasma-enhanced chemical vapor deposition for top cladding. We pattern the microheaters by e-beam lithography and sputter layers of 10 nm of titanium and 800 nm of aluminum, followed by a lift-off process in Acetone. We then spin SPR 220-7.0 photoresist and dice the wafer into mm-size chips. After a mild hard bake at 120 °C, we use xenon difluoride to etch away the silicon substrate near the tapers for efficient coupling. We estimate the response time of the microheaters to be less than 30 μs based on COMSOL heat transfer simulations. Our thermal tuning was fast enough to lock the ICL to the microring repeatedly to the same lasing wavelength because the lasing wavelength of the self-injection locked ICL is mainly determined by the gain medium, Fabry–Perot modes of the ICL, and the tuning of
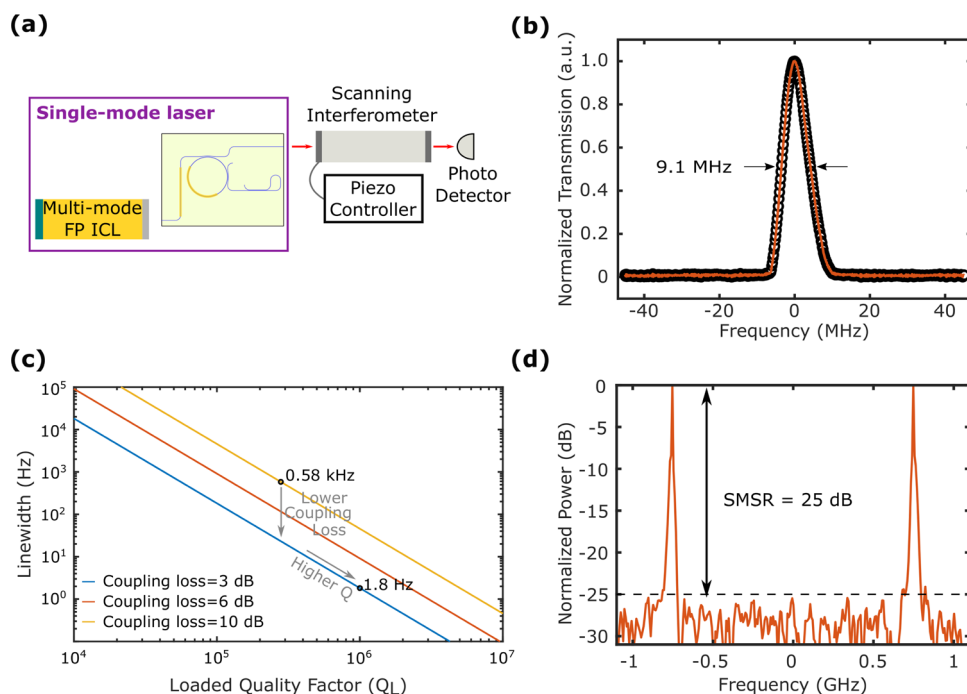
Fig. 6 Linewidth and side mode suppression ratio (SMSR) of the locked-state laser. a Linewidth measurement setup. **b** Measured linewidth of 9.1 MHz limited by the resolution of the scanning Fabry–Perot (FP) interferometer. **c** Calculated fundamental linewidth versus loaded quality factor (Q_L) for 0.4 mW output power. About two orders of magnitude improvement can be achieved with higher Q_L of the microresonator and improved coupling between the Interband Cascade Laser (ICL) and the silicon chip. **d** Measured SMSR of 25 dB. The FP interferometer resonance is scanned over one free-spectral range (FSR) with a piezoelectric controller.

Table 1 Performance metrics of chip-scale Interband Cascade Lasers near 3.0 µm.

	Operation mode	Lasing wavelength	Tuning range	Power variation over tuning range	Linewidth	Power	Side mode suppression ratio (SMSR)	Operating temperature
Ojanen et al.[24]	Multi-mode	2.59 µm	70 nm	7 dB	Not measured	<10 µW	14 dB	20 °C (range unspecified)
Yang et al.[8]	Single mode	2.81 µm	60 nm	10 dB	Not measured	1 mW	28 dB	−188 to −173 °C
Thorlabs (ID3250HHLH)	Single mode	3.25 µm	2.1 nm	6.5 dB	Not measured	5 mW	20 dB	15 to 35 °C
Alpes Lasers (CW-DFB-ICL 2946 cm⁻¹)	Single mode	3.39 µm	12 nm	Not available	Not measured	2 mW	25 dB	−20 to 40 °C
Our work	Single mode	3.40 µm	54 nm	3 dB	9 MHz (upper bound)	0.4 mW	25 dB	22 to 23 °C

the microring mode. Thus, when one of the ring resonances is tuned closer to one of the ICL modes, lasing at a particular wavelength can repeatedly be achieved, at least within the scanning FP interferometer resolution.

Experimental setup. We couple the output beam of the ICL to the bus waveguide on a silicon chip using a pair of aspheric lenses that are transparent in the mid-IR. The ICL operates in continuous-wave mode with threshold electrical pump and optical output values of 1.2 W and 0.4 mW, respectively. The aspheric lenses are made of black diamond-2 ($Ge_{28}Sb_{12}Se_{60}$) with broadband anti-reflection coating for the 3–5 µm wavelength range. A 1550 nm beam and the output beam of the multi-mode ICL are co-aligned through a pair of irises. Once the telecom beam is coupled to the chip using an IR camera, the mid-IR beam is also aligned to the chip. The coupling loss from the ICL to the input horn taper of the chip is approximately 10 dB.

To obtain spectral data, the output of the silicon chip is sent to an optical spectrum analyzer after an aspheric lens for beam collimation. The optical spectrum spectral resolution was 4.0 GHz (equivalent to 0.15 nm in wavelength), limited by the optical spectrum analyzer. We also co-align a tunable OPO with a linewidth of approximately 100 kHz through the chip and send its output to a photodetector connected to an oscilloscope for characterizing the linewidth of the microresonator. The cavity length of the ICL is 4 mm and the group index is 3.85 (values from Thorlabs). This yields the FSR of 19.48 GHz $\left(\text{FSR} = \frac{c}{n_g L} = 19.48\,\text{GHz}\right)$ which is 60 times larger than the resonator linewidth of 323 MHz. For all experiments we measure the output from the mirroring through-port. To measure the linewidth of the locked-state laser, we couple the output beam to a scanning Fabry–Perot interferometer (1.5 GHz FSR, 9 MHz resolution) controlled by a piezo-controller.

Estimation of linewidth. When the laser is self-injection locked to the micro-resonator, we expect a linewidth reduction from the free-running laser linewidth according to the ref. [10]

$$\Delta\nu_{\text{locked}} \approx \Delta\nu_{\text{free}} \frac{Q_{\text{ICL}}}{Q_{\text{Ring}}} \frac{1}{16\eta^2 R(1+\alpha^2)} \qquad (1)$$

where $\Delta\nu_{\text{locked}}$ and $\Delta\nu_{\text{free}}$ are the linewidth of the laser in the locked and free-running state, respectively. The quality factors Q_{ICL} and Q_{Ring} are those of the ICL and ring resonator, respectively. We estimate the ICL quality factor Q_{ICL} as $Q_{\text{ICL}} \approx \frac{2\pi\nu\tau R_{\text{ICL}}}{1 - R_{\text{ICL}}^2}$ where τ is the ICL cavity round trip and R_{ICL} is the reflection coefficient (amplitude) from the front facet of the ICL. We estimate the Q_{ICL} to be 3.1×10^3. The parameter R is the reflection from the Sagnac loop mirror that reflects about 10% of light to the laser diode. In addition, we have assumed an ICL linewidth enhancement factor of $\alpha \approx 2.2$, similar to the reference[23]. With these values, the estimated linewidth reduction factor is $\frac{\Delta\nu_{\text{locked}}}{\Delta\nu_{\text{free}}} \approx 1.3\times 10^{-3}$. To estimate the linewidth of the locked-state laser, we calculate the linewidth of the free-running ICL using the well-known modified Schawlow–Townes formula

$$\Delta\nu_{\text{free}} \approx \frac{1+\alpha^2}{4\pi P_{\text{ICL}}} K_{\text{tot}} n_{\text{sp}} (h\nu) v_g^2 \alpha_m (\alpha_m + \alpha_s) \qquad (2)$$

where K_{tot} is the total enhancement factor, n_{sp} is the population inversion factor, and v_g is the group velocity of the ICL. Considering the output power $P_{\text{out}} \approx 0.4\,\text{mW}$ and coupling efficiency $\eta \approx 10\,\text{dB}$, we estimate the linewidth of the free-running state ICL as $\Delta\nu_{\text{free}} \approx 0.45\,\text{MHz}$, giving the estimated linewidth of the locked-state laser $\Delta\nu_{\text{locked}} \approx 580\,\text{Hz}$.

Reporting summary. Further information on research design is available in the Nature Research Reporting Summary linked to this article.

Data availability

The data that support the findings of this study are available from the corresponding authors on reasonable request.

References

1. Tittel, F. K., Richter, D. & Fried, A. Mid-Infrared Laser Applications in Spectroscopy. In Solid-State Mid-Infrared Laser Sources (eds. Sorokina, I. T. & Vodopyanov, K. L.) 458–529 (Springer, 2003). https://doi.org/10.1007/3-540-36491-9_11
2. Lu, Q. Y., Bai, Y., Bandyopadhyay, N., Slivken, S. & Razeghi, M. 2.4 W room temperature continuous wave operation of distributed feedback quantum cascade lasers. *Appl. Phys. Lett.* **98**, 181106 (2011).

3. Yang, R. Q. et al. Distributed Feedback Mid-IR Interband Cascade Lasers at Thermoelectric Cooler Temperatures. *IEEE J. Sel. Top. Quantum Electron.* **13**, 1074–1078 (2007).
4. Bismuto, A. et al. High power and single mode quantum cascade lasers. *Opt. Express, OE* **24**, 10694–10699 (2016).
5. Lyakh, A., Barron-Jimenez, R., Dunayevskiy, I., Go, R. & Patel, C. K. N. External cavity quantum cascade lasers with ultra rapid acousto-optic tuning. *Appl. Phys. Lett.* **106**, 141101 (2015).
6. Maulini, R., Mohan, A., Giovannini, M., Faist, J. & Gini, E. External cavity quantum-cascade laser tunable from 8.2 to 10.4 μm using a gain element with a heterogeneous cascade. *Appl. Phys. Lett.* **88**, 201113 (2006).
7. Chevalier, P. et al. Watt-level widely tunable single-mode emission by injection-locking of a multimode Fabry-Perot quantum cascade laser. *Appl. Phys. Lett.* **112**, 061109 (2018).
8. Yang, H., Yang, R. Q., Yang, R. Q., Gong, J. & He, J.-J. Mid-infrared widely tunable single-mode interband cascade lasers based on V-coupled cavities. *Opt. Lett., OL* **45**, 2700–2703 (2020).
9. Stern, B., Ji, X., Dutt, A. & Lipson, M. Compact narrow-linewidth integrated laser based on a low-loss silicon nitride ring resonator. *Opt. Lett., OL* **42**, 4541–4544 (2017).
10. Kondratiev, N. M. et al. Self-injection locking of a laser diode to a high-Q WGM microresonator. *Opt. Express, OE* **25**, 28167–28178 (2017).
11. Gil-Molina, A. et al. Robust Hybrid III-V/Si3N4 Laser with kHz-Linewidth and GHz-Pulling Range. In *Conference on Lasers and Electro-Optics (2020)*, paper STu3M.4 (Optical Society of America, 2020). https://doi.org/10.1364/CLEO_SI.2020.STu3M.4
12. Stern, B., Ji, X., Okawachi, Y., Gaeta, A. L. & Lipson, M. Battery-operated integrated frequency comb generator. *Nature* **562**, 401–405 (2018).
13. Raja, A. S. et al. Electrically pumped photonic integrated soliton microcomb. *Nat. Commun.* **10**, 680 (2019).
14. Borri, S. et al. Whispering gallery mode stabilization of quantum cascade lasers for infrared sensing and spectroscopy. in *Laser Resonators, Microresonators, and Beam Control XIX* vol. 10090 1009008 (International Society for Optics and Photonics, 2017).
15. Chen, L. & Lipson, M. Ultra-low capacitance and high speed germanium photodetectors on silicon. *Opt. Express, OE* **17**, 7901–7906 (2009).
16. Reboud, V. et al. Germanium based photonic components toward a full silicon/germanium photonic platform. *Prog. Cryst. Growth Charact. Mater.* **63**, 1–24 (2017).
17. Gorodetsky, M. L., Pryamikov, A. D. & Ilchenko, V. S. Rayleigh scattering in high-Q microspheres. *J. Opt. Soc. Am. B, JOSAB* **17**, 1051–1057 (2000).
18. Galiev, R. R. et al. Spectrum collapse, narrow linewidth, and Bogatov effect in diode lasers locked to high-Q optical microresonators. *Opt. Express, OE* **26**, 30509–30522 (2018).
19. Liang, W. et al. Ultralow noise miniature external cavity semiconductor laser. *Nat. Commun.* **6**, 7371 (2015).
20. Miller, S. A. et al. Low-loss silicon platform for broadband mid-infrared photonics. *Optica* **4**, 707–712 (2017).
21. Griffith, A. G. et al. Silicon-chip mid-infrared frequency comb generation. *Nat. Commun.* **6**, 6299 (2015).
22. Yu, M., Okawachi, Y., Griffith, A. G., Lipson, M. & Gaeta, A. L. Mode-locked mid-infrared frequency combs in a silicon microresonator. *Optica* **3**, 854–860 (2016).
23. Deng, Y., Zhao, B.-B., Wang, X.-G. & Wang, C. Narrow linewidth characteristics of interband cascade lasers. *Appl. Phys. Lett.* **116**, 201101 (2020).
24. Ojanen, S.-P. et al. GaSb diode lasers tunable around 2.6 μm using silicon photonics resonators or external diffractive gratings. *Appl. Phys. Lett.* **116**, 081105 (2020).

Acknowledgements

Author contributions

E.S. designed and fabricated the devices, performed the measurements, and prepared the manuscript. A.G. and O.W. aided the design and measurements. Y.D. and K.L. provided the ICL with an anti-reflective coated facet. M.L. and A.L.G. supervised the research. E.S., A.G., O.W., A.L.G., and M.L. edited the manuscript.

Competing interests

The authors declare no competing interests.

Additional information